International Journal of Heat and Mass Transfer 52 (2009) 4500–4509

Contents lists available at ScienceDirect

International Journal of Heat and Mass Transfer

journal homepage: www.elsevier.com/locate/ijhmt

Flow maldistribution and thermal performance deterioration in a cross-flow air to air heat exchanger with plate-fin cores

Li-Zhi Zhang *

Key Laboratory of Enhanced Heat Transfer and Energy Conservation of Education Ministry, School of Chemistry and Chemical Engineering, South China University of Technology, Guangzhou 510640, China

ARTICLE INFO

Article history:
Received 26 December 2008
Received in revised form 6 March 2009
Accepted 16 March 2009
Available online 11 May 2009

Keywords:
Heat transfer
Flow maldistribution
Compact heat exchanger
Plate-fin

ABSTRACT

The inlet and outlet duct geometry in an air to air compact heat exchanger is always irregular. A skewed *Z*-type arrangement is popular between the impinging flow and the core. Such duct placements usually lead to a non-uniform flow distribution on core surface. In this research, the flow maldistribution and thermal performance deterioration in cross-flow air to air heat exchangers are investigated. The inlet duct, the core and the outlet duct are combined together to calculate the flow distribution on core inlet face. First, a CFD code is used to calculate the flow distribution, by treating the plate-fin core as a porous media. Then a heat transfer model between the two air flows in the plate-fin channels is set up. Using the flow distribution data predicted, the heat exchange effectiveness and the thermal performance deterioration factor are calculated with finite difference scheme. Experiments are performed to validate the flow distribution and heat transfer model. The results indicate that when the channel pitch is below 2.0 mm, the flow distribution is quite homogeneous and the thermal deterioration due to flow maldistribution can be neglected. However, when the channel pitch is larger than 2 mm, the maldistribution is quite large and a 10–20% thermal deterioration factor could be found. The study proves that the inlet duct, the outlet duct, and the core should be coupled together to clarify flow maldistribution problems.

1. Introduction

Air to air heat exchangers have been widely used in air conditioning industry for heat recovery from ventilation air. Fig. 1 shows the schematic of a typical commercialized air to air heat exchanger-the so called heat recovery ventilator. As seen, the whole exchanger is composed of inlets, outlets, exchanger shells, separating plates, and most importantly, the core. When installed, the exchanger core is rotated 45° and inserted into the exchanger shell, forming two parallel air ducts with the separating plates in the rectangular shell box. Fresh air is sucked into the exchanger by a fan (not shown in the figure) through the fresh air inlet. Exhaust air is sucked into the exchanger by another fan through the exhaust air inlet. The two air streams are drawn through the exchanger core in a cross-flow arrangement. The structure of the exchanger core is shown in Fig. 2. It is a plate-fin structure to have extended surfaces. The structures depicted by Figs. 1 and 2 are popular and typical, because they are compact, easy in installation, replacement and maintenance.

Fluid flow and heat transfer in such an exchanger are of interests to predict energy recovery efficiencies. The effectiveness-Number of Transfer Units (ε-*NTU*) method has been the most convenient methodology to predict performance. Fluid flow and heat transfer in a single core channel provides the basic transport data for effectiveness-*NTU* methodology. There have been numerous investigations of the heat transfer and fluid flow in a single plate-fin channel. Duct cross-sections are the predominant factor influencing pressure drop and heat transfer coefficients. Ducts of various crosssections like parallel-plates, triangles, and sinusoidal shapes were calculated both experimentally and numerically [1–7].

Even though a single core channel has been investigated in detail, the fluid flow and heat transfer in a whole exchanger have not been studied sufficiently. Considering the complex ducting work inside a practical exchanger shell, it is anticipated that the flow would undergo turnarounds, expansions and contractions, which would finally lead to flow maldistribution across the core face. However, almost all these previous studies concentrated only on a representative single channel in the exchanger core, by neglecting the real flow distribution in the whole exchanger. In other words, a uniform flow distribution across the core face was assumed. This is certainly a very ideal assumption which needs further clarification.

The flow maldistribution effects have been well recognized and presented for heat exchangers and cooling towers. For plate heat exchangers, Bassiouny and Martin [8,9] analytically calculated the axial velocity and pressure distribution in both the intake and exhaust conduits of plate heat exchangers. One-dimensional flow distribution for both the *U*-type and the *Z*-type arrangements

* Tel./fax: +86 20 87114268.
E-mail address: Lzzhang@scut.edu.cn

0017-9310/$ - see front matter © 2009 Elsevier Ltd. All rights reserved.
doi:10.1016/j.ijheatmasstransfer.2009.03.049

Nomenclature

a	half channel pitch (m)
A	Area (m^2)
b	channel width (m)
c_p	specific heat (kJ kg^{-1} K^{-1})
D_h	hydrodynamic diameter (m)
f	channel friction factor
G	mass flow rate (kg/s)
h	convective heat transfer coefficient (k Wm^{-2} K^{-1})
$\dot{m}$	mass flow rate (kg m^{-2} s^{-1})
n	number of channels for each flow
NTU	Number of Transfer Units
Nu	Nusselt number
P	pressure (Pa)
Re	Reynolds number
S	source term
T	temperature (K)
u_d	duct velocity (m/s)
u_i	face velocity (m/s)
V	volumetric flow rate (m^3/h)
x	coordinate (m)
x_F	channel length (m)
y	coordinate (m)
y_F	channel length (m)
z	coordinate (m)
z_F	core depth (m)

Greek letters

ρ	density (kg/m^3)
ε	effectiveness
β	flow nonuniformity
λ	heat conductivity (Wm^{-1} K^{-1})
α	permeability (m^2)
τ	thermal performance deterioration factor
δ	thickness (μm)
μ	viscosity (kg m^{-1} s^{-1})
Ω	fin conductance parameter

Superscripts

*	dimensionless

Subscripts

a	air
e	exhaust air
f	fresh air
fin	fins
i	inlet
m	mean
o	outlet
p	plate

are obtained. The flow maldistribution is due to flow branching and the consequent momentum change. Based on their findings, Rao et al. [10] further investigated the effect of flow distribution to the channels on the thermal performance of a plate heat exchanger. Dwivedi and Das [11] then studied the transient behavior of plate heat exchangers with port to channel maldistribution. For crossflow compact heat exchangers, Shah [12] studied the deterioration of heat exchanger performance due to one-dimensional flow non-uniformity. Ranganayakulu et al. [13] calculated the two-dimensional flow distribution across the exchanger core after the inlet duct. The flow maldistribution is generated by the velocity profiles in the inlet ducts. Their effects on heat transfer were estimated. Other studies involving modeling flow and heat transfer in air to air heat exchangers include [14–18].

The aforementioned studies provided some insight into the effects of inlet duct on flow maldistribution on core surface. However, there were some flaws in previous studies. First, the real inlet duct geometry in the shell is much more irregular and complex. A heat exchanger as shown in Fig. 1 is much more complex than an ideal rectangular pipe as assumed in refs [8,9,13]. Second, the incoming fluids impinge on the core surface with an angle, not in normal directions. So the arrangement here is neither *U*-type nor

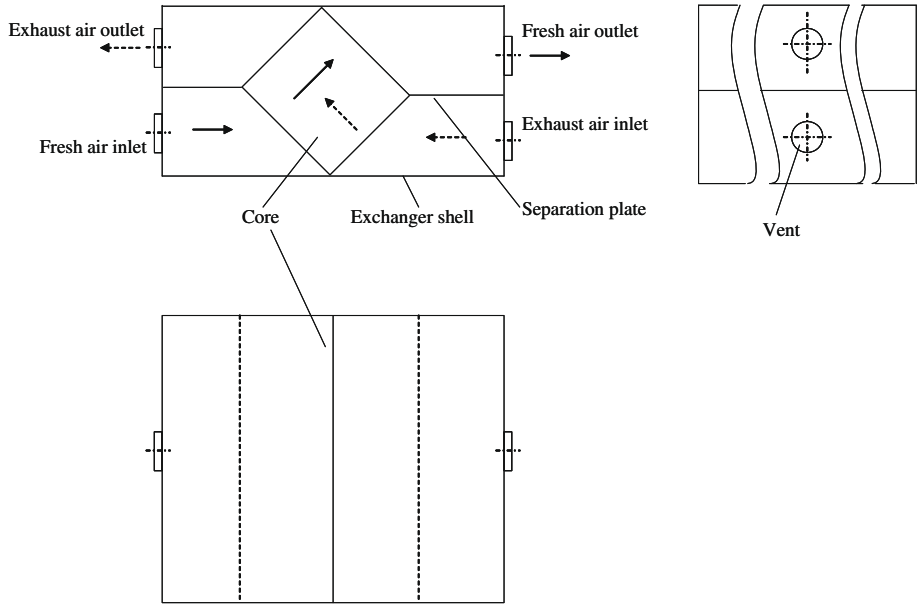

Fig. 1. Schematic of a cross-flow air to air heat exchanger.

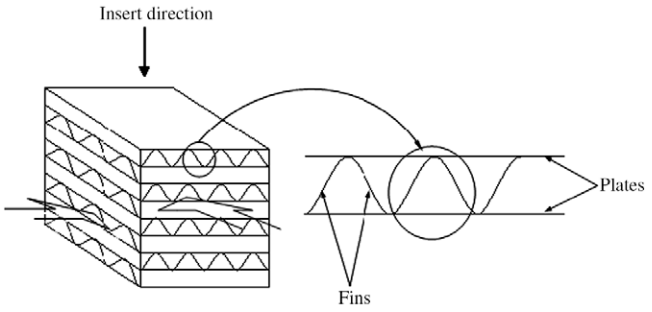

Fig. 2. Schematic of the heat exchanger core, with plate-fin structure.

Z-type, but a three-dimensional skewed *Z*-type. Third, previous studies solved the velocity distribution in the inlet duct without the coupling with the core. They separated the inlet duct from the core and did not consider the effects of core when solving the fluid fields in the inlet duct. In other words, the inverse effects of core on flow distribution in the conduits were not reflected. This may lead to unrealistic (or too ideal) flow distribution in the exchanger, considering the strong interactions between the inlet conduits, the core and the outlet conduits.

To have a more realistic and accurate analysis, a different approach will be taken in this study. The flow maldistribution will be calculated by selecting the whole exchanger as the domain. The influences of inlet duct, the core and the outlet duct will be considered simultaneously. After the maldistribution of flow fields are obtained, their effects on thermal performance of the heat exchanger will be discussed.

2. Theoretical work

2.1. Flow maldistribution prediction

The fluid flow in the exchanger is numerically calculated. The fresh air duct and the exhaust air duct are in symmetry. So only the fresh air duct as shown in Fig. 3 is selected as the calculating domain. There have been several numerical studies concerning the modeling of flow maldistribution in plate heat exchangers, on a channel to channel basis [18–20]. However, due to the limit in computer capacity and speed, the number of channels that can be modeled directly is quite small. Miura et al. [14] modeled the flow maldistribution in a simple 2 channel heat exchanger. Galeazzo et al. [19] modeled the flow variations in a four channel heat exchanger. Bansode et al. [20] modeled the flow distribution among four proton exchange membrane cells. They are detailed enough to disclose local variations in a channel. However, a real core usually has hundreds of channels. The large number of channels phases out the direct simulation of flow on a channel to channel basis. To solve this problem, this study simulates the core as a porous media, which only permits one dimensional air flow along the channel length. The methodology is reasonable, considering the small channel pitch (1.5–5 mm) in the core. The honeycomb type core structure permits the assumption of unmixed flow for both of the fluids, in other words, cross or transverse mixing of fluids is not considered. When modeling the fluid flow, heat transfer is not considered. In other words, isothermal flow in one stream is considered.

Due to the complex geometry, a commercial CFD code is employed. The computational grids are generated with the software GAMBIT and the problem is numerically solved using the finite volume method with the software FLUENT. The whole geometry comprises of three parts: the inlet duct, the core and the outlet duct. The geometrical properties are listed in Table 1. The geometrical parameters are different. Air passes through inlet vent, inlet duct, the core, outlet duct, and the outlet vent, consecutively. The inlet duct and the outlet duct are air flow in a volume. The core is treated as a porous media. The fluid domains are modeled with air at room temperature. The boundary condition at the outlet vent is the volumetric flow rate leaving the outlet vent surface. The boundary condition at the inlet vent is "outflow", which means a zero axial variable gradients across the outlet vent surface. This is because air is sucked inside from the inlet vent. Other surfaces are defined as wall conditions, except the two core surfaces facing and backing the air flow (surface $x^* = 0$ and 1). A laminar model is used since air velocity inside the core is usually small, in the order of 1 m/s. Second order discretization of all variables is employed, and the simulation is considered converged when the residual of all variables remained below 10^{-4} and the mean inlet velocities remained constant.

A view of the mesh structure can be seen in Fig. 4. They are mixed structure meshes including both structured and unstructured meshes. The grid sensitivity of the results is checked compar-

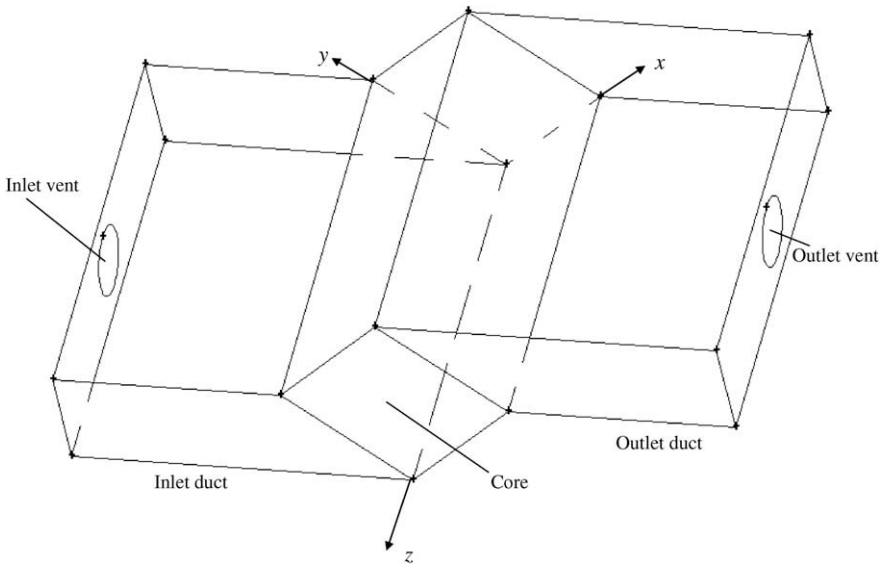

Fig. 3. The calculating domain for fresh air flow.

Table 1
Structural and physical parameters of the two cores tested.

Symbol	Unit	Core A	Core B
n		92	127
x_F, y_F	mm	185	185
z_F	mm	460	460
δ_{fin}, δ_p	μm	100	100
λ_{fin}, λ_p	$Wm^{-1}K^{-1}$	237	237
a/b		0.4	0.4
$2a$	mm	2.5	1.8
D_h	mm	2.15	1.55
A_p	m^2	6.30	8.69
A_f, A_e	m^2	14.62	20.16
Ω		450.3	450.3
Nu		2.12	2.12
$f\bullet$Re		44.8	44.8
Inlet/outlet duct length	mm	262	262
Inlet/outlet vent diameter	mm	60	60

ing the results of two grids with different refinement levels. The coarse grids configurations have approximately 160,387 cells (97,751 tetrahedral cells and 62,638 hexahedral cells), while the fine grids have approximately 230,668 cells (102,355 tetrahedral cells and 128,313 hexahedral cells). The mean absolute difference between the results with the coarse and fine grids is below 1%. As the results show negligible grid sensitivity, the coarse grid is used in the rest of this work to speed up convergence.

The core is defined as a porous media. The porous media model can be used for a wide variety of problems, including flows through packed beds, filter papers, perforated plates, flow distributors, and tube banks. The porous media model incorporates an empirically determined flow resistance in a region of the model defined as 'porous'. In essence, the porous media model is nothing more than an added momentum sink in the governing momentum equations. Porous media are modeled by the addition of a momentum source term to the standard fluid flow equations. The source term is composed of two parts, a viscous loss term (Darcy), and an inertial loss term, as expressed as

$$S_i = \sum_{j=1}^{3} D_{ij}\mu u_j + \sum_{j=1}^{3} C_{ij}\frac{1}{2}\rho|u_j|u_j \tag{1}$$

where S_i is the source term for the ith (x, y, or z) momentum equation, and D and C are prescribed matrices. This momentum sink contributes to the pressure gradient in the porous cell, creating a pressure drop that is proportional to the fluid velocity (or velocity squared) in the cell.

To recover the case of simple homogeneous porous media

$$S_i = \frac{\mu}{\alpha}u_i + C_2\frac{1}{2}\rho|u_i|u_i \tag{2}$$

where α is the permeability and C_2 is the inertial resistance factor, simply specify D and C as diagonal matrices with $1/\alpha$ and C_2, respectively, on the diagonals (and zero for the other elements).

In laminar flows through porous media, the pressure drop is typically proportional to velocity and the constant C_2 can be considered to be zero. Ignoring convective acceleration and diffusion, the porous media model then reduces to Darcy's Law. The pressure drop across the channel can be calculated by

$$\Delta P = \frac{\mu}{\alpha}u_i\Delta x \tag{3}$$

where u_i is the face velocity in the core (in x direction).

Based on the definition of friction factor for ducts [1,2], we have

$$\Delta P = \frac{\Delta x}{D_h}f\frac{1}{2}\rho u_d^2 \tag{4}$$

$$\mathrm{Re} = \frac{\rho u_d D_h}{\mu} \tag{5}$$

where u_d is velocity in ducts. It is twice the face velocity, because half the core face is blocked and sealed for the other passage.

$$u_d = 2u_i \tag{6}$$

For fully developed laminar flow in ducts [1,2],

$$(f\cdot\mathrm{Re}) = C_3 \tag{7}$$

where C_3 is a constant for a given crosssection. For instance, C_3 is 64 for round tube; 96 for parallel plates; 53.2 for isosceles triangular duct with an aspect ratio of 0.5; 44.8 for sinusoidal duct with an aspect ratio of 0.4. The values of C_3 for other duct crosssectional ducts can be found in Ref. [1,2].

Substituting Eq. (4) through Eq. (7) to Eq. (3), the permeability can be calculated by

$$\alpha = \frac{D_h^2}{C_3} \tag{8}$$

As seen, when the core structure is known, its equivalent permeability can be evaluated by above equation. Its effects on flow distribution can then be calculated. The value of $1/\alpha$ can be input

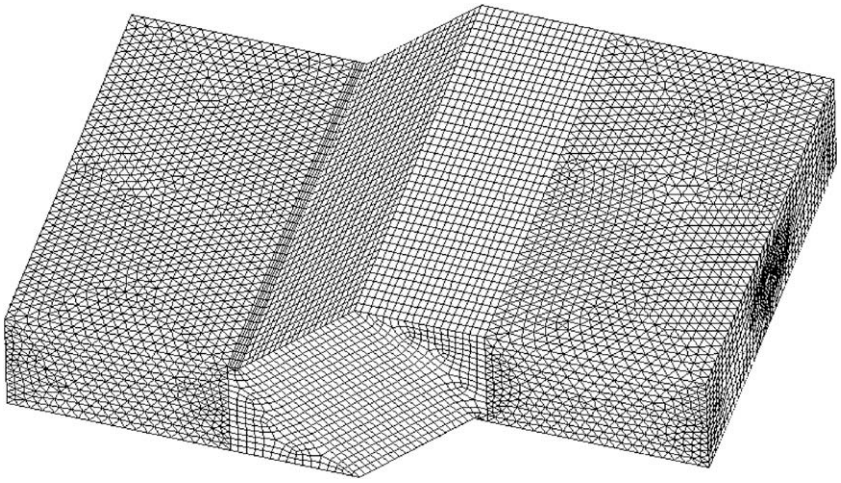

Fig. 4. The mesh generated for the CFD modeling.

into the software directly. Since the fluid can only flow in the channel length direction (x), the permeability in other two directions are set to infinitely small.

With the method described above, the fluid flow in the whole exchanger can be calculated. The two dimensional velocity distributions on the core face ($x^* = 0$) can be predicted. The maldistribution can be analyzed with a definition of local flow nonuniformity parameter as

$$\beta = \frac{\dot{m}}{\dot{m}_m} \tag{9}$$

where $\dot{m}$ is the actual local mass flow rate ($kg\,m^{-2}\,s^{-1}$), and $\dot{m}_m$ is the average mass flow rate across the core face. When the air is considered as incompressible fluid, the nonuniformity can be simply calculated as the local to mean velocity ratio.

2.2. Heat transfer model in cores

After the flow distribution on the core face is known, the convective heat transfer between the fresh air and the exhaust air can be studied. To aid in the model set up, following assumptions are made: (1) the flow distribution inside a channel is taken to be uniform giving a 'plug flow' of fluid inside each channel. It can be justified as the channel gap is small. (2) The flow in channels is fully developed both hydradynamically and thermally. For fully developed laminar flow in ducts with well conductive walls, the Nusselt number is a constant once the crosssection is determined. Therefore the convective heat transfer coefficient is also a constant. (3) The plates are considered to be thin enough so that axial conduction in them in the direction of flow can be neglected. (4) The thermophysical properties of the fluids are considered to be independent of temperature and pressure.

A meso-scopic model is set up. Each channel crosssection is represented by one temperature. The temperature varies along flow directions (x for fresh air and y for exhaust air) and the corresponding perpendicular directions (y for fresh air and x for exhaust air) simultaneously. On each channel crosssection, though temperature is two-dimensionally different locally, in this study for the whole exchanger, they are represented by a lumped parameter for each channel crosssection. It can be considered as a semi-lumped parameter model. The two air streams, one hot (fresh air), and the other cool (exhaust air), exchange heat in the exchanger in a cross-flow arrangement. Two-dimensional heat transfer model can be set up to govern the energy conservations in the two air streams [21]:

$$\frac{\partial T_f^*}{\partial x^*} = NTU_f(T_{pf}^* - T_f^*) \tag{10}$$

$$\frac{\partial T_e^*}{\partial y^*} = NTU_e(T_{pe}^* - T_e^*) \tag{11}$$

where x is flow direction for fresh stream and y is flow direction for exhaust stream. Certainly, since the local mass flow rate is variant with both core height (y direction) and core depth (z direction), the local number of transfer units are different from point to point on the core surface.

The dimensionless temperature is defined by

$$T^* = \frac{T - T_{ei}}{T_{fi} - T_{ei}} \tag{12}$$

The dimensionless coordinates are defined by

$$x^* = \frac{x}{x_F} \tag{13}$$

$$y^* = \frac{y}{y_F} \tag{14}$$

$$z^* = \frac{z}{z_F} \tag{15}$$

where x_F and y_F are channel lengths for fresh air and exhaust air (m). Here $x_F = y_F$. Core depth, which determines the total number of channels, is z_F. The air side local number of transfer units is defined by

$$NTU_f = \frac{1}{\beta}\frac{(hA)_f}{(Gc_p)_f} \tag{16}$$

$$NTU_e = \frac{1}{\beta}\frac{(hA)_e}{(Gc_p)_e} \tag{17}$$

where h is air side convective heat transfer coefficient ($k\,Wm^{-2}\,K^{-1}$); G is total air mass flow rate across the whole core for a stream (kg/s); A is total transfer area including plates and fins (m^2) for each stream; c_p is specific heat ($kJ\,kg^{-1}\,K^{-1}$). Subscripts "f" refers to fresh side and "e" refers to exhaust side; "pf" refers to plate surface on fresh side, and "pe" refers to plate surface on exhaust side.

As seen, in Eqs. (16) and (17), the last term in the right hand side is the overall number of transfer units for a stream. The local number of transfer unit is equal to the overall number of transfer units divided by the local to overall mass flow ratio. Therefore, the local number of transfer units is inversely proportional to mass flow ratio. Local number of transfer units increases with decreased mass flow rate.

The convective heat transfer coefficient can be calculated by

$$Nu = \frac{hD_h}{\lambda_a} \tag{18}$$

where λ_a is heat conductivity of air ($k\,Wm^{-1}\,K^{-1}$). For plate-fin channels of finite fin conductance, the fully developed Nusselt numbers are influenced by aspect ratios (a/b), and fin conductance parameters [10].

The fin conductance parameter for sensible heat transfer

$$\Omega = \frac{\lambda_{fin}\delta_{fin}}{\lambda_a(2a)} \tag{19}$$

where λ_{fin} is heat conductivity of fin, δ_{fin} is fin thickness (m), and ($2a$) is channel height or pitch (m).

Heat conduction through the plate is in equilibrium with the convective heat transfer on both sides. The equilibrium can be expressed by

$$(hA)_f(T_f^* - T_{pf}^*) = \frac{A_p\lambda_p}{\delta_p}(T_{pf}^* - T_{pe}^*) \tag{20}$$

$$(hA)_e(T_e^* - T_{pe}^*) = -\frac{A_p\lambda_p}{\delta_p}(T_{pf}^* - T_{pe}^*) \tag{21}$$

where A_p is total transfer area (m^2) of plates; λ_p is heat conductivity of plate ($k\,Wm^{-1}\,K^{-1}$); δ_p is thickness of plate (m). In above two equations, the right hand sides are heat conduction through plates. They have the same value, but different signs. In the left hand sides, the first equation represents convective heat transfer in fresh air side, and the second equation represents convective heat transfer in exhaust air side.

Heat exchanger effectiveness

$$\varepsilon = \frac{(Gc_p)_f(T_{fi} - T_{fo})}{(Gc_p)_{min}(T_{fi} - T_{ei})} = \frac{(Gc_p)_e(T_{eo} - T_{ei})}{(Gc_p)_{min}(T_{fi} - T_{ei})} \tag{22}$$

When the two streams have the same mass flow rate

$$\varepsilon = \frac{(T_{fi} - T_{fo})}{(T_{fi} - T_{ei})} = \frac{(T_{eo} - T_{ei})}{(T_{fi} - T_{ei})} = T_{eo}^* \tag{23}$$

The exchanger thermal performance deterioration factor is defined by

$$\tau = \frac{\varepsilon_{uniform} - \varepsilon}{\varepsilon_{uniform}} \tag{24}$$

where $\varepsilon_{uniform}$ is exchanger effectiveness at uniform flow distribution.

Boundary conditions

Fresh:

$$T_f^*|_{x^*=0} = 1 \quad (25)$$

Exhaust:

$$T_e^*|_{y^*=0} = 0 \quad (26)$$

2.3. Solution procedure

A finite difference technique is used to discrete the partial differential equations developed for the air streams. The calculating domain of core is divided into a number of discrete nodes. Each node represents a control volume. The number of calculating node is 50 in both x direction and y direction. Besides the discretisation of energy equation in x and y directions, the whole core depth is divided into 100 cells (z direction). Under this scheme, it is like that the whole core is divided into 100 mini cross-flow heat exchangers in core depth. For each mini cross-flow heat exchanger, the inlet velocity varies with y direction for fresh air and x direction for exhaust air, respectively.

An upstream differencing scheme is used for two air streams. The two air streams and the plate are closely coupled in heat transfer. Therefore, iterative techniques are needed to solve these equations. A description of the iterative procedure is as following:

(a) Calculate the mass flow rate distribution on core inlet faces ($x^* = 0$, and $y^* = 0$), based on the resistance of the core.
(b) Assume initial temperature fields in the two streams.
(c) Calculate the temperature values on plate surfaces by Eqs. (20) and (21).
(d) Taking the current values of temperature on plate surfaces as the default values, get the temperature profiles in two air streams by solving Eqs. (10) and (11). Substituting the local mass flow rate distribution obtained in (a) into the equations for both the fresh air and the exhaust air.
(e) Go to (c), until the old values and the newly calculated values of temperature at all calculating nodes are converged.

After these procedures, all the governing equations are solved simultaneously. To assure the accuracy of the results presented, numerical tests were performed for the core to determine the effects of the grid size. It indicates that 50 grids are adequate (less than 0.1% difference compared with 80 grids) for z and y direction, and 100 grids are adequate for z direction. The final numerical uncertainty is 0.1%.

When the temperature fields in the exchanger core are calculated, the heat exchange effectiveness is calculated using mean outlet values on outlet face of $x^* = 1$ or $y^* = 1$. These are numerically obtained data.

3. Results and discussion

3.1. Experimental validation

To measure the heat exchange effectiveness, several experiments are done. A schematic of the test rig is shown in Fig. 5. Two air ducts are assembled. One is for fresh air, and the other is for exhaust air. Each duct comprises of a variable speed sucking blower, a wind tunnel, a set of nozzles, wind straighteners, and temperature sensors before and after the exchanger. The exchanger is connected to the two ducts with flanges. The whole test rig is established in a constant temperature and constant humidity room, so the inlet temperature of the exhaust air, which equals to the room air, can be controlled and maintained very well even under very hot and humid ambient weather conditions. Additional electric heating circuits are installed for the fresh air duct. The heating power currents can be adjusted according to the fresh air set points temperature. A 10 mm thick plastic foam insulation layer is pasted on the outer surfaces of the ducts and the exchanger shells to prevent heat dissipation from the system to the surroundings. The heat loss from the system is below 0.5%.

The nominal operating conditions: fresh air inlet 35 °C; exhaust air inlet 27 °C. During the experiment, equal air flow rates are kept for the two ducts. The design air flow rates are 150 m^3/h. In the test, they are changed by variable speed blowers, to have different air velocities. Temperature and volumetric flow rates are monitored at the inlet and outlet of the exchanger. Before and after each test, temperature sensors are calibrated with a Pt-100 temperature sensor. Hot-wire anemometers that are used to measure the wind speed before and after the exchanger are compared with the air flow rates measured by nozzles. The offset is controlled to within 1% limit. Volumetric air flow rates are varied from 100 to 200 m^3/h, corresponding to frontal air velocities from 0.37 to 0.74 m/s which are typical for commercial heat exchangers. Air flow under such conditions is laminar, with Reynolds numbers not exceeding 200. The uncertainties are: temperature ±0.1 °C; volumetric flow rate ±1%. The final uncertainty is ±4.5% for exchanger effectiveness. The fresh air and exhaust air temperature change differences are controlled to be less than 0.1%. From these preparatory works, the test rig is considered to be reliable. In addition, heat balance between the fresh air and the exhaust air are checked.

After the measurement of mean inlet and outlet temperature, the exchanger effectiveness can be calculated with Eq. (22). This is the experimentally obtained effectiveness.

Besides the measurement of inlet and outlet mean temperatures of the whole exchanger, local velocities and temperatures are also monitored through the data sampling holes drilled on the exchanger

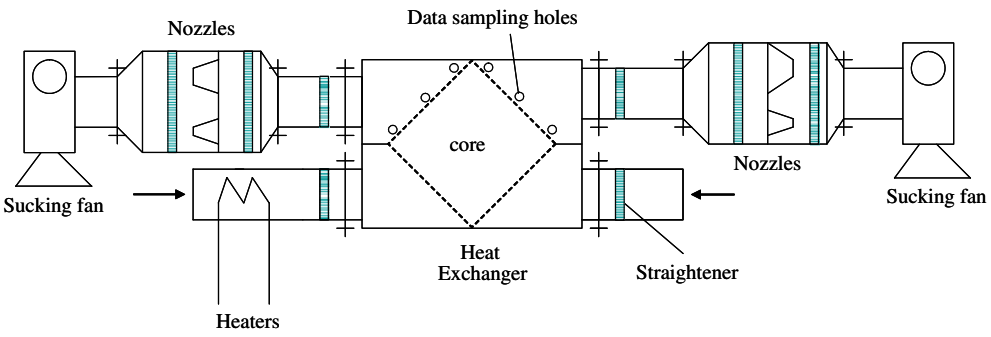

Fig. 5. Experimental set-up of the heat exchanger.

shells, as depicted in Fig. 5. Temperature sensors or hot-wire anemometers can be inserted into the holes to probe the parameters near the outlet face of the core. The purpose is to validate the flow and temperature distribution fields calculated with the model. Totally nine points are monitored on the outlet face. The positions of the nine points (Position A–I) are shown in Fig. 6.

Two cores are obtained and tested. They are plate-fin structure with sinusoidal duct crosssection. They are made with aluminum foils as the plate and fin materials. The core depths are the same: 460 mm. Core A has 92 channels, and core B has 127 channels for each stream. The channel pitch for core A is 2.5 mm, and the channel pitch for core B is 1.8 mm. The geometrical and transport properties have been listed in Table 1.

The heat exchange effectiveness of the two cores inserted in the exchanger shell under various volumetric air flow rates are plotted in Fig. 7. The measured data are demonstrated by discrete dots. The calculated data are plotted by a solid line. The maximum deviation between the calculated value and the measured data is below 5%, indicating the performance is predicted satisfactorily. Due to the compact structure and the high packing density, the heat transfer area is very large. Therefore, the exchanger effectiveness is rather high. The outside dimensions are then same, but Core A has 92 passages and core B has 127 passages. Core B is more compact than core A, so the effectiveness of core B is higher than core A.

The fresh air duct and the exhaust air duct have the same flow distribution. The local velocities on fresh air outlet ($x^* = 1$) are measured through the data sampling holes on fresh air duct. At the same time, local temperatures on exhaust air outlet ($y^* = 1$) are monitored through the data sampling holes on exhaust air duct. The data sampling points for temperature have the same definition as in Fig. 6, but y axis is replaced by x axis. The temperatures and the velocities are measured directly first, then they are transformed to dimensionless, for ease in comparison. The local velocities are transformed to velocity nonuniformity based on Eq. (9) and the temperatures are transformed to dimensionless temperatures based on Eq. (12). Both the calculated data and the measured values are listed in Table 2. As seen, the predictions are generally well. The difference of velocity is less than 8% and the disparity of temperature is less than 4.8%. It can be observed from this table that the velocity maldistribution on core A is much higher than that on Core B. The highest nonuniformity is 2.33 on Core A, but only 1.24 on Core B. This indicates that the flow maldistribution on Core A is very serious, but the flow maldistribution on core B is negligible. The higher the local mass flow rates are, the less the local outlet temperature is. The methodology and the mathematical model are accurate enough to predict the performance of the heat exchanger with flow maldistribution. The precision for velocity is 0.001 m/s.

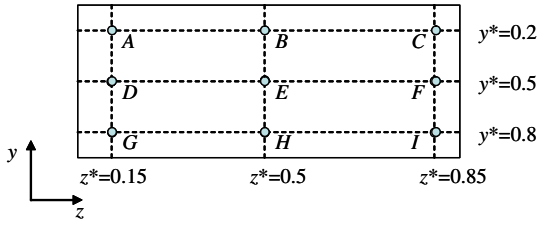

Fig. 6. The positions of data sampling points on the plane 1 mm above the core outlet face.

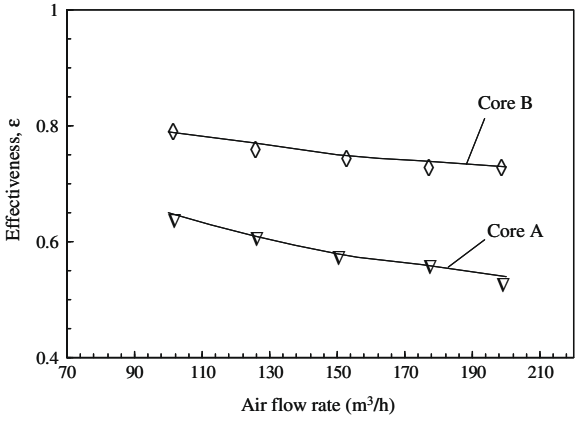

Fig. 7. Heat exchange effectiveness of the two plate-fin cores under various air flow rates. The solid line is the calculated values, and the discrete dots are the measured data.

3.2. Flow maldistribution

The effects of the core channel pitch on flow maldistribution are modeled. Three channel pitches are considered: 1.8 mm (B), 2.5 mm (A), and 4 mm (C). The core dimensions and other structural parameters are fixed as in Table 1. The profiles of velocity nonuniformity on core outlet face for the three pitches are plotted in Figs. 8–10. The total volumetric air flow rate for each stream is 150 m^3/h, which equals to a mean face velocity 0.49 m/s or mean duct velocity 0.98 m/s. The flow distributions on the core inlet face are the same as those on outlet face, since only one dimensional flow on channel length is permitted.

As seen from these figures, a general rule can be concluded: the larger the channel pitch is, the more serious the flow maldistribution is. The maximum flow nonuniformity for 4.0 mm pitch core is 3.11, while only 1.234 for 1.8 mm pitch core. For all cores, the highest velocity exists at the center of the core face where the incoming fluids impinge on the core directly. The least velocity exists on the corners of the core surface, because here the pressure is the least. As expected, the nonuniformity is symmetric to the plane $z^* = 0.5$ due to geometric symmetry. However, due to the skew angle between the core face and the impinge flow, the nonuniformity is asymmetric to plane $y^* = 0.5$. These results indicate that the flow maldistribution is co-determined by the inlet duct, the core and the outlet duct. The core itself plays a determinant role in the flow maldistribution. These components should be coupled together to predict the flow maldistribution. The previous methodology of separating the core from the inlet duct has problems. Further, when the core channel pitch is below 2 mm, a uniform flow distribution can be assumed. This is easy to understand. A core with such small channels is just like a flow straightener. Flow after such equipments becomes uniform. On the other hand, flow maldistributions on cores with channel pitches larger than 2 mm are very serious. They should be taken into account.

The values of pressure drop illustrate this phenomenon. Table 3 lists the calculated pressure drop for three cores with channel pitch 1.8 mm (B), 2.5 mm (A) and 4.0 mm (C), respectively. The smaller the channel is, the higher the pressure drop is. For the 1.8 mm pitch, the pressure drop across the core accounts for 45% of the total heat exchanger pressure drop. For the 4.0 mm channel pitch core, the core pressure drop only accounts for 3% of the total pressure drop. Therefore for the large channel pitch cores, the flow distribution is mainly determined by inlet duct geometry since core resistance is negligible.

Velocity vectors on plane $y^* = 0.5$ are plotted in Fig. 11. The plane is cut at the center of the core. The channel pitch is 2.5 mm and flow rate is 150 m^3/h. As seen, the incoming air impinges on the core face and some flow is driven by the core face to the remote areas at corners. There are swirls generated before

Table 2
Local values of velocity nonuniformity and dimensionless temperature under V=150m^3/h.

Points	Velocity nonuniformity, β				Dimensionless temperature, T^*			
	Core A		Core B		Core A		Core B	
	Calculated	Tested	Calculated	Tested	Calculated	Tested	Calculated	Tested
A	1.156	1.234	0.954	0.967	0.634	0.625	0.949	0.917
B	2.616	2.533	1.264	1.235	0.562	0.547	0.921	0.897
C	1.156	1.245	0.954	0.936	0.634	0.618	0.949	0.913
D	0.418	0.425	0.917	0.924	0.561	0.581	0.79	0.782
E	2.451	2.331	1.2	1.243	0.473	0.493	0.755	0.738
F	0.418	0.423	0.917	0.928	0.561	0.598	0.79	0.779
G	0.41	0.432	0.971	0.983	0.522	0.552	0.569	0.582
H	2.06	2.241	1.272	1.293	0.424	0.434	0.549	0.558
I	0.41	0.442	0.971	0.956	0.522	0.509	0.569	0.588

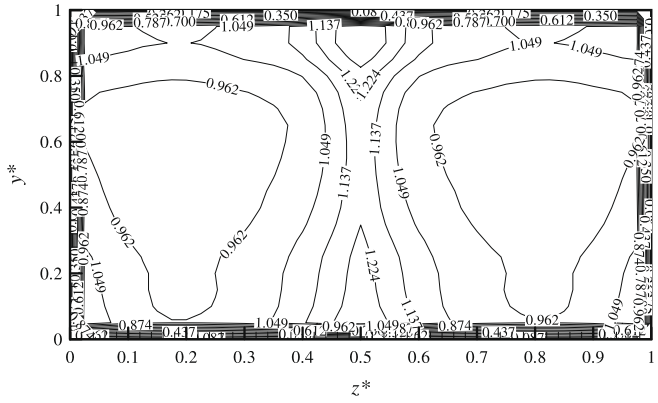

Fig. 8. Velocity nonuniformity on core face, channel pitch = 1.8 mm.

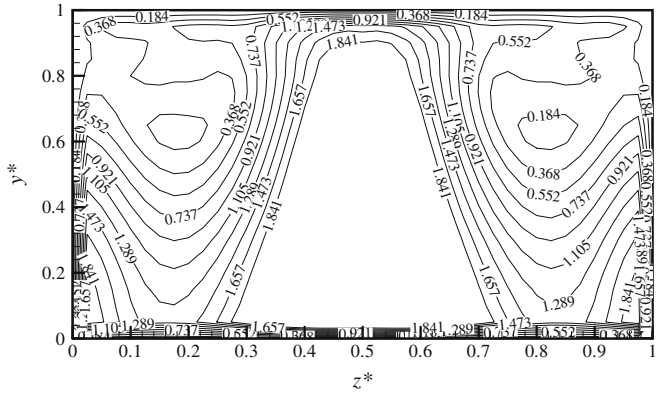

Fig. 9. Velocity nonuniformity on core face, channel pitch = 2.5 mm.

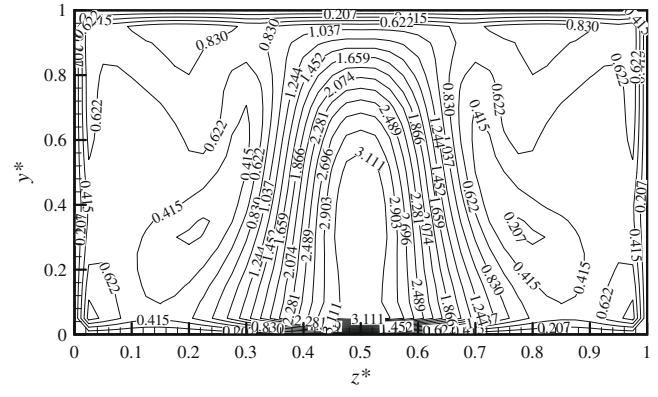

Fig. 10. Velocity nonuniformity on core face, channel pitch = 4.0 mm.

Table 3
Pressure drop for the three exchangers.

Channel pitch (mm)	1.8		2.5		4	
V (m^3/h)	150	250	150	250	150	250
Whole exchanger (Pa)	102.9	234.8	64.5	179.2	63.6	178.1
Core (Pa)	46.7	77.9	5.8	8.7	1.9	3.9

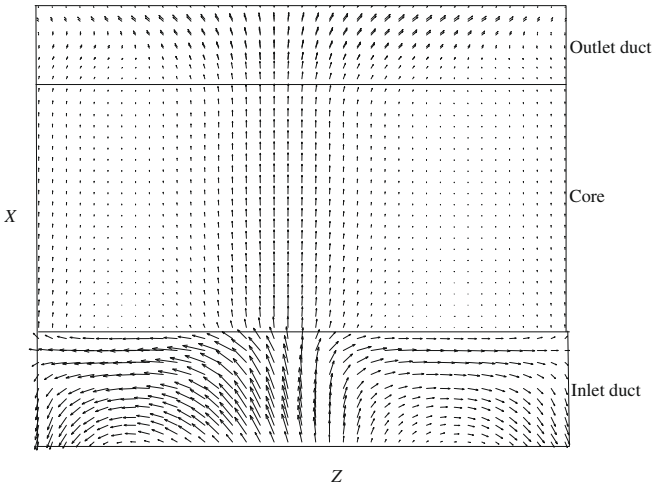

Fig. 11. Velocity vectors on plane y^* = 0.5 (center plane in core).

the core face, which lead to flow re-distribution. The flow in the core becomes somewhat uniform, due to this re-distribution. The higher the core resistance is, the more serious the swirls are, and the more homogeneous the flow redistributes.

Velocity also has an influence on flow nonuniformity. The flow nonuniformity for 2.5 mm channel pitch under air flow rate 250 m^3/h is plotted in Fig. 12. Comparing Fig. 12 and Fig. 9, it can be concluded that the shapes of flow nonuniformity are similar. However, the values are somewhat different. The higher the total air flow rates are, the more inhomogeneous the flow becomes. In Fig. 12, the nonuniformity at the face center becomes larger, but those near the corners become less. At higher air flow rates, the flow maldistribution becomes more serious.

3.3. Thermal performance analysis

With the heat transfer model, the local temperature on outlet face of the core can be calculated. Let we assume that the whole exchanger is divided into a number of mini exchangers in z direction. Each mini heat exchanger is an x–y cross-flow heat exchanger. The outlet temperatures for each mini exchanger vary with x or y

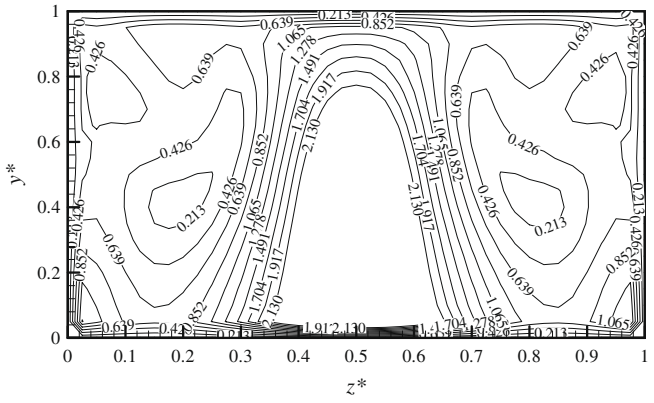

Fig. 12. Velocity nonuniformity on core face, channel pitch = 2.5 mm, $V = 250 m^3/h$.

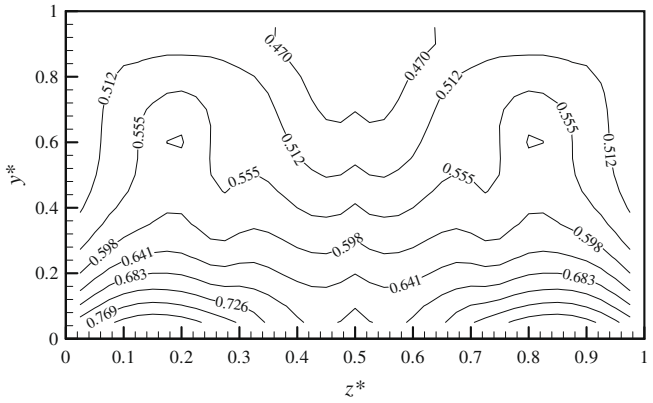

Fig. 14. Local heat exchange effectiveness, channel pitch = 2.5 mm.

directions. Therefore, outlet temperature for fresh air is two-dimensional on z–y face, while outlet temperature for exhaust air is two-dimensional on z–x face. As indicated in Eq. (23), the dimensionless outlet temperature of exhaust air T^*_{eo} represents an effectiveness for local heat exchanger. We call this effectiveness the local effectiveness, representing a channel to channel local heat exchanger efficiency.

Figs. 13–15 show the local effectiveness for the three cores of different channel pitches: 1.8 mm (B), 2.5 mm (A), and 4.0 mm (C). As seen, for the homogeneous flow distribution on 1.8 mm core (B), the local effectiveness iso-lines are nearly parallel to plates, meaning the divided mini exchangers in core depth have the same local effectiveness. Both the flow and heat transfer are uniform in core depth. The flow is uniform in y direction, but the local effectiveness is in the opposite. This is due to the cross-flow heat exchange between the fresh air and the exhaust air, as in other common cross-flow heat exchangers.

When the maldistribution becomes serious with increased channel pitches, the local effectiveness becomes irregular. Generally, the higher the local velocity is, the less the local effectiveness is. At the same time, the local effectiveness is also influenced by the temperature difference between the two neighboring fresh air and exhaust air. This results in a phenomenon that the local effectiveness curves for 4.0 mm core is more complex than that for 1.8 mm core.

For engineering applications, the overall effectiveness of the whole exchanger is more significant. Fig. 16 depicts the exchanger thermal performance deterioration factor under various air flow rates for the three cores. As can be seen, the thermal performance

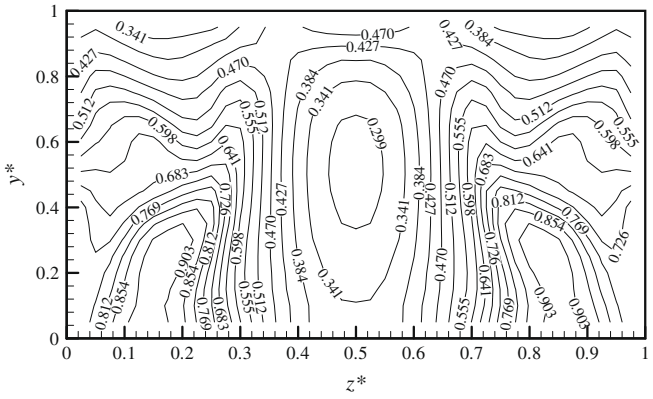

Fig. 15. Local heat exchange effectiveness, channel pitch = 4.0 mm.

deterioration factor for the 1.8 mm (B) core is very small and the performance deterioration can be neglected. However, for the two cores with larger channel pitches (A and C), the performance deteriorations are substantial. The thermal effectiveness is deteriorated by 10–20%. The more serious the maldistribution is, the worse the performance is.

4. Conclusions

Flow maldistribution is a result of interactions between inlet duct flow, flow in cores and flow in outlet duct. The core itself plays

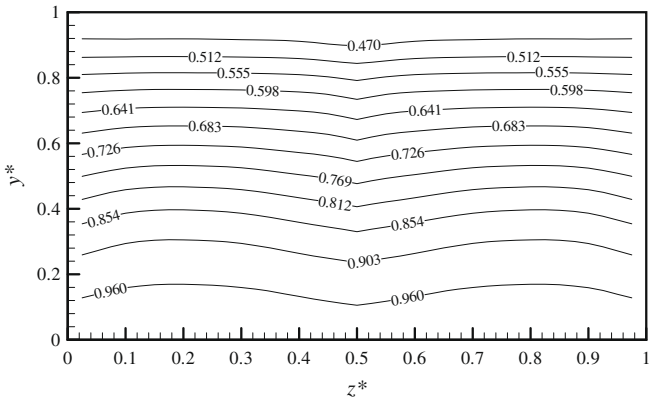

Fig. 13. Local heat exchanger effectiveness, channel pitch = 1.8 mm.

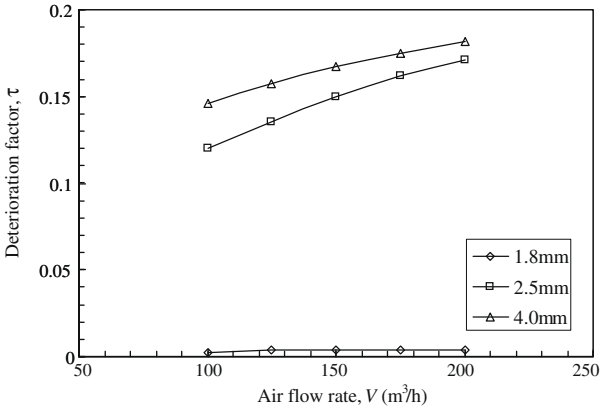

Fig. 16. Thermal performance deterioration factor for the three cores.

a determining role in flow distribution. Previous studies have failed to reflect this phenomenon. A detailed numerical modeling and experiment is performed to study the flow maldistribution and its effect on thermal deterioration. Following results can be found:

(1) For plate-fin compact heat exchanger cores, the channel pitch determines how serious the flow maldistribution is. When the channel pitch is less than 2 mm, the flow maldistribution is very small and can be neglected. When the channel pitch is larger than 2 mm, the flow maldistribution becomes serious and the nonuniformity problem should be considered.
(2) Local heat exchange effectiveness is inversely proportional to local mass flow rate. For the cores with larger channel pitches, flow maldistribution generated thermal deterioration factors can be as high as 10–20%.
(3) The cores of small pitches have larger pressure resistance, which could offset some degree of flow maldistribution that is generated by irregular duct geometries like turnaround, expansion, and contraction.

Acknowledgements

This Project 50676034 is supported by National Natural Science Foundation of China. The project is also supported by the National High Technology Research and Development Program of China (863), 2008AA05Z206.

References

[1] R.K. Shah, A.L. London, in: Laminar Flow Forced Convection in Ducts, Academic Press Inc., New York, 1978, pp. 253–260.
[2] F.P. Incropera, D.P. Dewitt, Introduction to Heat Transfer, 3rd ed., vol. 8, John Wiley & Sons, New York, 1996, p. 416.
[3] R.K. Shah, M.S. Bhatti, Laminar convection heat transfer in ducts, in: S. Kakac, R.K. Shah, W. Aung (Eds.), Handbook of Single-Phase Convective Heat Transfer, Wiley, New York, 1987.
[4] S. Chen, T.L. Chan, C.W. Leung, Numerical prediction of laminar forced convection in triangular ducts with unstructured triangular grid method, Numer. Heat Trans. A 38 (2000) 209–224.
[5] B.R. Baliga, R.R. Azrak, Laminar fully developed flow and heat transfer in triangular plate-fin ducts, ASME J. Heat Trans. 108 (1986) 24–32.
[6] L.Z. Zhang, Thermally developing forced convection and heat transfer in rectangular plate-fin passages under uniform plate temperature, Numer. Heat Trans. A Appl. 52 (2007) 549–564.
[7] L.Z. Zhang, Laminar flow and heat transfer in plate-fin triangular ducts in thermally developing entry region, Int. J. Heat Mass Trans. 50 (2007) 1637–1640.
[8] M.K. Bassiouny, H. Martin, Flow distribution and pressure drop in plate heat exchangers-I, *U*-type arrangement, Chem. Eng. Sci. 39 (1984) 693–700.
[9] M.K. Bassiouny, H. Martin, Flow distribution and pressure drop in plate heat exchangers-II, *Z*-type arrangement, Chem. Eng. Sci. 39 (1984) 701–704.
[10] B.P. Rao, P.K. Kumar, S.K. Das, Effect of flow distribution to the channels on the thermal performance of a plate heat exchanger, Chem. Eng. Process. 41 (2002) 49–58.
[11] A.K. Dwivedi, S.K. Das, Dynamics of plate heat exchangers subject to flow variations, Int. J. Heat Mass Trans. 50 (2007) 2733–2743.
[12] R.K. Shah, Flow maldistribution-compact heat exchangers, in: W.M. Rohsenow, P.J. Hartnett, E.N. Ganic (Eds.), Handbook of Heat Transfer Applications, McGraw-Hill, New York, 1985, pp. 266–280.
[13] Ch. Ranganayakulu, K.N. Seetharamu, K.V. Sreevatsan, The effects of inlet fluid flow nonuniformity on thermal performance and pressure drops in cross-flow plate-fin compact heat exchangers, Int. J. Heat Mass Trans. 40 (1997) 27–37.
[14] R.Y. Miura, F.C.C. Galeazzo, C.C. Tadini, J.A.W. Gut, The effect of flow arrangement on the pressure drop of plate heat exchangers, Chem. Eng. Sci. (2008), doi:10.1016/j.ces.2008.07.029.
[15] E. M Sparrow, J.C.K. Tong, J.P. Abraham, Fluid flow in a system with separate laminar and turbulent zones, Numer. Heat Trans. A 53 (2008) 341–353.
[16] H. Pingaud, J.M. Le Lann, B. Koehret, Steady-state and dynamic simulation of plate fin heat exchangers, Comput. Chem. Eng. 13 (1989) 577–585.
[17] K. Nakoniec, Numerical modeling of cross-flow plate-fin air-to-air heat exchanger under unsteady flow conditions, Numer. Heat Trans. A 49 (2006) 1–24.
[18] P. Yuan, Effect of inlet flow maldistribution on the thermal performance of a three-fluid cross-flow heat exchanger, Int. J. Heat Mass Trans. 46 (2003) 3777–3787.
[19] F.C.C. Galeazzo, R.Y. Miura, J.A.W. Gut, C.C. Tadini, Experimental and numerical heat transfer in a plate heat exchanger, Chem. Eng. Sci. 61 (2006) 7133–7138.
[20] A.S. Bansode, S. Patel, T.R. Kumar, B. Muralidhar, T. Sundararajan, S.K. Das, Numerical simulation of effects of flow maldistribution on heat and mass transfer in a PEM fuel cell stack, Heat Mass Trans. 43 (2007) 1037–1047.
[21] L.Z. Zhang, C.H. Liang, L.X. Pei, Heat and moisture transfer in application-scale parallel-plates enthalpy exchangers with novel membrane materials, J. Membr. Sci. 325 (2008) 672–682.